HHS Public Access

Author manuscript

J Pain. Author manuscript; available in PMC 2022 June 01.

Published in final edited form as:

J Pain. 2021 June ; 22(6): 692–706. doi:10.1016/j.jpain.2020.12.006.

A role for protease activated receptor type 3 (PAR3) in nociception demonstrated through development of a novel peptide agonist

Juliet Mwirigi[1,*], **Moeno Kume**[1,*], **Shayne N Hassler**[1,*], **Ayesha Ahmad**[1], **Pradipta R Ray**[1], **Changyu Jiang**[2], **Alexander Chamessian**[2], **Nakleh Mseeh**[1], **Breya P Ludwig**[1], **Benjamin D. Rivera**[4], **Marvin T Nieman**[3], **Thomas Van de Ven**[2], **Ru-Rong Ji**[2], **Gregory Dussor**[1], **Scott Boitano**[4], **Josef Vagner**[5], **Theodore J Price**[1,#]

[1]University of Texas at Dallas, School of Behavioral and Brain Sciences and Center for Advanced Pain Studies

[2]Duke University School of Medicine, Depts. of Anesthesiology, Pharmacology, and Cancer Biology

[3]Case Western Reserve University School of Medicine, Department of Pharmacology

[4]University of Arizona, Department of Physiology; Asthma and Airway Disease Research Center

[5]University of Arizona, Bio5 Research Institute

Abstract

The protease activated receptor (PAR) family is a group of G-protein coupled receptors (GPCRs) activated by proteolytic cleavage of the extracellular domain. PARs are expressed in a variety of cell types with crucial roles in hemostasis, immune responses, inflammation, and pain. PAR3 is the least researched of the four PARs, with little known about its expression and function. We sought to better understand its potential function in the peripheral sensory nervous system. Mouse single-cell RNA sequencing data demonstrates that PAR3 is widely expressed in dorsal root ganglion (DRG) neurons. Co-expression of PAR3 mRNA with other PARs was identified in various DRG neuron subpopulations, consistent with its proposed role as a coreceptor of other PARs. We developed a lipid tethered PAR3 agonist, C660, that selectively activates PAR3 by eliciting a Ca^{2+} response in DRG and trigeminal (TG) neurons. *In vivo*, C660 induces mechanical hypersensitivity and facial grimacing in WT but not $PAR3^{-/-}$ mice. We characterized other

[#]Corresponding author: Theodore J Price, University of Texas at Dallas, School of Behavioral and Brain Sciences, 800 W Campbell Rd, BSB 14.102, Richardson TX 75080, 972-883-4311, Theodore.price@utdallas.edu.

[*]equal contribution

AUTHOR CONTRIBUTIONS

Performed experiments: JM, MK, SNH, AA, PRR, CJ, AC, NM, BPL, BDR

Analyzed data: JM, MK, SNH, AA, PRR, CJ, RRJ, JV, TJP

Contributed novel reagents: MTN, JV

Wrote the paper: JM, MK, SNH, TJP

Edited the paper: PRR, MTN, TVdV, RRJ, GD, SB, JV

nociceptive phenotypes in PAR3$^{-/-}$ mice and found a loss of hyperalgesic priming in response to IL-6, carrageenan, and a PAR2 agonist, suggesting that PAR3 contributes to long-lasting nociceptor plasticity in some contexts. To examine the potential role of PAR3 in regulating the activity of other PARs in sensory neurons, we administered PAR1, PAR2, and PAR4 agonists and assessed mechanical and affective pain behaviors in WT and PAR3$^{-/-}$ mice. We observed that the nociceptive effects of PAR1 agonists were potentiated in the absence of PAR3. Our findings suggest a complex role of PAR3 in the physiology and plasticity of nociceptors.

Graphical Abstract

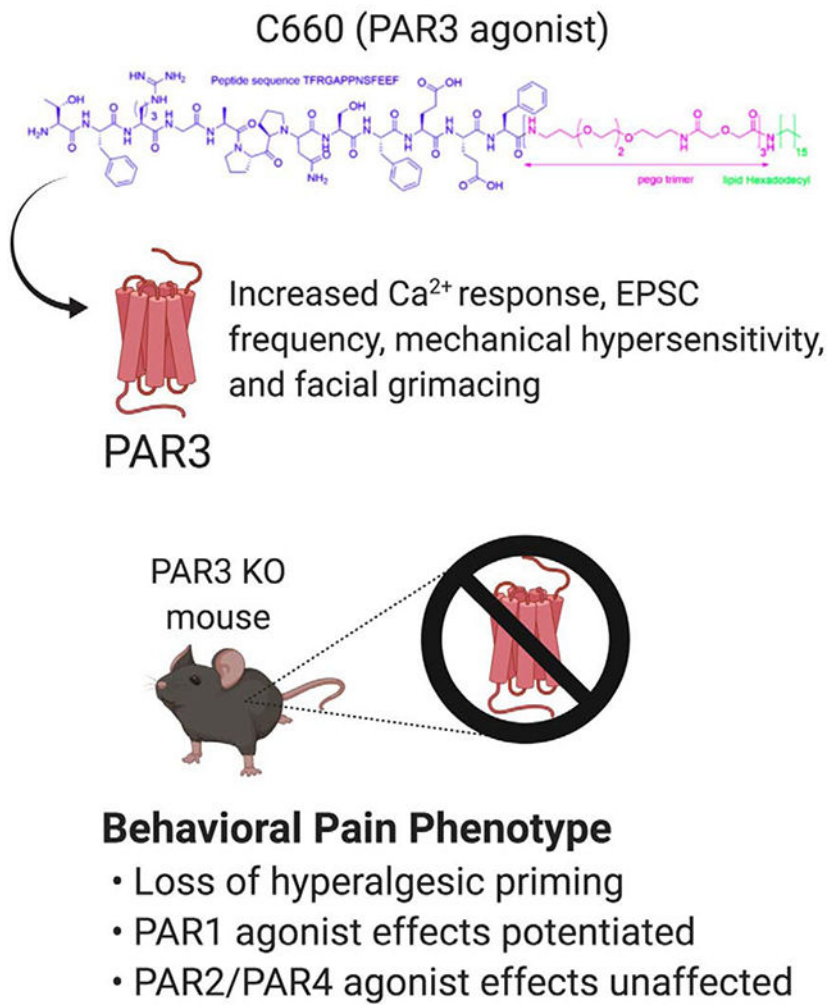

Keywords

PAR3; protease activated receptor; nociceptor; pain; hyperalgesic priming

INTRODUCTION

Protease activated receptor 3 (PAR3) belongs to the PAR family of G-protein coupled receptors (GPCRs), a group of receptors expressed in many cell types and implicated in a

variety of inflammatory pathologies [11, 26, 28, 56]. Like the other PARs, PAR3 does not have an endogenously present ligand but rather is activated through extracellular cleavage of the N-terminal end via proteases. After proteolytic cleavage, the newly available tethered ligand can bind to the receptor, initiating multiple downstream signaling cascades [51]. In contrast to the other PARs, comparatively little research or drug development efforts have been made for PAR3 since its discovery in the 1990s as a second receptor for thrombin, a protease critical for the coagulation process [13, 19, 30]. PAR3, encoded by the *F2rl2* gene, is neuronally expressed [9, 66], but its physiological role in sensory neurons in the DRG or TG has not been assessed. PAR3 has been shown to regulate PAR1 signaling in endothelial cells and PAR4 signaling in platelets in response to thrombin [42, 47].

Significant roadblocks in PAR3 research have been the lack of specific agonists and skepticism on whether the receptor can signal autonomously. Early research showed that COS-7 cells transfected with human PAR3 stimulated with thrombin were able to trigger robust phosphoinositide signaling [30]. Murine PAR3, on the other hand, was unable to signal on its own in response to thrombin when transfected in COS-7 cells [47]. Studies using agonist peptides based on the tethered ligand sequence of PAR3 (TFRGAP and TFRGAPPNS) have yielded mixed results. TFRGAP elicited a Ca^{2+} response in rat astrocytes [60] and human smooth muscle cells [6]. However, it was later observed that TFRGAP induced extracellular regulated kinase (ERK) activation via PAR1 rather than PAR3 in human A-498 carcinoma cells and mouse lung fibroblasts [35]. Furthermore, studies with PAR3 tethered-ligand sequences have evidenced an inability of PAR3 to self-activate in the absence of other PARs [22, 30]. We recently described a lipid tethering approach to profoundly increase the potency of PAR agonist peptides [17]. We reasoned that the deployment of this approach for PAR3 could clarify how this receptor might signal in DRG neurons *in vitro* and *in vivo*.

In this study, we had several aims with the overarching goal of gaining better insight into the potential role of PAR3 in nociception. The first was to characterize PAR3 expression in mouse DRG. We find that *F2rl2* mRNA is widely expressed in nociceptors and overlaps with other PAR-expressing subpopulations. Second, we developed a lipid-tethered peptidomimetic agonist for PAR3 and evaluated its pharmacology *in vivo* and *in vitro*. Finally, we measured both mechanical and affective nociceptive effects of various PAR-mediated and non-PAR-mediated stimuli in $PAR3^{-/-}$ mice. Our findings highlight the role of PAR3 in regulating PAR1- evoked pain behaviors and hyperalgesic priming.

MATERIALS AND METHODS

Animals

8-week old mice, weighing between 20–25 grams, were used in this study. Strains include ICR (Taconic, Envigo), C57BL/6J (Jackson Laboratories), and $PAR3^{-/-}$ on a C57Bl6/J background (MMRRC, Chapel Hill, NC). The animals were housed in a climate-controlled room with a 12-hour light/dark cycle and given food and water *ad libitum*. All experiments and procedures were performed per the guidelines recommended by the National Institute of Health (NIH), the International Association for the Study of Pain (IASP). They were approved by the Institutional Animal Care and Use Committees at Duke University and the University of Texas at Dallas (license protocol number 14–04).

Experimental reagents

Compound 660 (TFRGAPPNSFEEF-pego3-Hdc), compound 661 (GAPPNSFEEF-pego3-Hdc), compound 662 (TFRGAP-pego3-Hdc), compound 663 (TFR-pego3-Hdc), AYPGKF-NH_2 (PAR4 activation peptide), 2-aminothiazo-4-yl-LIGRL-NH_2 (2AT), and other ligands (Supplemental Fig. S1B) were made using solid-phase synthesis as previously described [4, 16]. The full structure of C660 is depicted in Fig. 2A. Carrageenan, 48–80, thrombin, picrotoxin, strychnine, and TFLLR-NH_2 were purchased from Sigma-Aldrich, IL-6 was purchased from R&D Systems; Prostaglandin E_2 (PGE_2) was purchased from Cayman Chemicals. For behavioral testing, the listed reagents were administered intraplantarly using saline as the vehicle. Tetrodotoxin was from Tocris.

Design of tethered PAR3 ligands

Compound 660 (TFRGAPPNSFEEF-pego3-Hdc) represents the canonical sequence of peptide TFRGAPPNSFEEF, which stays tethered to the receptor activated by thrombin cleavage of the K38/T39 peptide bond in PAR3. The peptide is attached via a short trimeric pego linker to the lipid tail, which resembles lipids of the cell membrane. Compound 661 (GAPPNSFEEF-pego3-Hdc), compound 662 (TFRGAP-pego3-Hdc), compound 663 (TFR-pego3-Hdc), C737 (FEEF-pego3-Hdc), and C742 (NSFEEF-pego3-Hdc) are truncated analogs of C660. Compounds C728 (Ac-pego3-Hdc) and C729 (scrambled C660 peptide PGTEFNFARESFP-pego3-Hdc) are negative controls. Compound C733 (TFRGAPPNSFEEF-amide) represents the original peptide sequence without the pego linker and lipid anchor. Compound C741 (RTFRGAPPNSFEEF-pego3-Hdc) is the N-terminal Arg38 extension of C660. Finally, compound C751 (TFRGAPPNSFEEF-pego3-KLIPAIYLLVFVVGV-amide) and C752 (TFRGAPPNSFEEF-pego3-KRRPAIYLLVFVVGV-amide) are analogs of C660 consisting of the active sequence TFRGAPPNSFEEF connected to the original PAR3 transmembrane peptide K^{96}LIPAIYLLVFVVGV^{109} (Uniprot O00254) via a pego3 linker. We synthesized a ligand with full transmembrane domain K^{96}LIPAIYLLVFVVGVPANAVTLWMLF^{120}, but this ligand was not tested as the lipophilic TM domain induced very poor solubility. Even compound C751 suffers from low solubility in aqueous buffers. Therefore, we included two arginine residues, K^{96}<u>RR</u>PAIYLLVFVVGV^{109} (underlined), in the transmembrane interface of C752. The solubility of C752 improved; nonetheless, the compound was not active in RTCA.

RNAscope in situ hybridization and image analysis

For *in situ* hybridizations, trigeminal ganglia (TG) from C57BL/6J male mice were dissected and post-fixed for 2 hours at 4°C. TGs were cryo-sectioned to 12 μm, thaw-mounted onto Superfrost Plus (Fisher Scientific) slides, allowed to dry for 20 mins at RT, and then stored at −80°C. *In situ* hybridization was performed using the RNAscope system (Advanced Cell Diagnostics). Tissue pretreatment consisted of 30 minutes of Protease IV at RT, rather than the recommended procedure for fixed frozen tissue. Following pretreatment, probe hybridization and detection with the Multiplex Fluorescence Kit v2 were performed according to the manufacturer's protocol. Probes included Mm-F2rl2 (#489591), Mm-Trpv1-C2 (313331-C2), and Mm-Nefh-C3 (443671-C3). After detection, the tissues were

counterstained with DAPI (4',6-diamidino-2-phenylindole) and mounted with Prolong Gold (Life Technologies). Fluorescence was detected using an epifluorescence microscope (Nikon Eclipse NiE).

20X images of TGs were acquired using the Nikon Eclipse NiE. Six sections of the left and right TGs were imaged per mouse (n=4). Images were analyzed on Olympus Cell Sens (v1.18) for the expression of *F2rl2*, *Trpv1,* and *Nefh*. Images were first brightened and contrasted before counting the number of cells using the point tool. Total neuron counts were made for *Nefh* positive cells and all cells outlined by DAPI. *F2rl2*-positive neurons were then counted (including cells with less than five puncta) and illustrated as a percentage of the total neuronal count on a pie chart. *F2rl2 was* also evaluated for co-expression with *Trpv1* in TG neurons.

Evaluation of C660-induced PAR3 signaling in vitro

Real-time monitoring of PAR3 response to C660 was assessed by measuring electrical impedance using the xCELLigence Real-Time Cell Analyzer (ACEA Biosciences, San Diego, CA) as previously described for PAR2 compounds [17]. Briefly, media were placed in 96-well gold electrode-coated plates (E-plates; ACEA Biosciences) to obtain background signal. PAR3 was stably expressed using the HEK293 Flp-In T-Rex cells according to the manufacturer's protocol (Invitrogen) as has been described for PAR4[21]. HEK293 cells grown initially at 37°C in a 5% CO_2 atmosphere at 70% confluence were treated with tetracycline (0.3 μg/mL or 1 μg/mL) for 48 hrs to induce PAR3 expression. Cells (180 μL) were transferred in low serum medium (DMEMF12; 5% FBS) onto Poly-L-Lysine coated E-plates and monitored for Cell Index (CI) using the xCELLigence real-time cell analyzer (RTCA; ACEA Biosciences). CI is dimensionless and is calculated by $CI = (Z_i - Z_0)/15\ \Omega$, where Z_i is the impedance at an individual time point during the experiment, Z_0 is the impedance at the start of the experiment, and Ω represents ohms. This relative change in electrical impedance represents physiological cell status in response to signaling; cell status can be affected by changes in cell morphology, adhesion, or viability. At CI stabilization (approximately 6 hrs after plating), 20 μL of 10× final concentration C660 (in DMEMF12) was added to each well for a final 1× concentration in a volume of 200 μL. Assays included both induced and non-induced cells treated with varying concentrations of C660 in quadruplicate. CI was measured after C660 addition every minute for 4 hrs. Peak changes in CI after C660 addition were used to determine the dose-response to C660 within an individual E-plate. These responses were normalized as percentages of the peak response within each plate to determine EC_{50}s from multiple plates, as previously described [17]. Individual traces of the CI over time shown in Fig. 2 represent the average of a quadruplicate from a single E-plate.

Behavioral methods

8-week old male mice were used for all the behavioral tests shown in Fig. 4–8 and Supplementary Fig. S2–S5. Experiments were also performed in 8-week old female mice, as shown in Supplementary Fig. S6.

The protocol initially developed by Mogil and colleagues for testing facial grimacing in mice was adapted for this study. The same cohorts of mice were used to assess facial grimacing[39] and mechanical withdrawal thresholds. Mice were placed individually on a tabletop in cubicles (9×5×5 cm high) with two walls of transparent acrylic glass and two side walls of removable stainless steel. To record facial expressions of the mice, two high-resolution (1920×1080) digital video cameras (High-definition Handycam Camcorder, model HDR-CX100, Sony, San Jose, CA) were placed immediately outside both acrylic glass walls to maximize the opportunity for precise headshots. The mice were then recorded for 20 minutes, and the photographs that included views of the mouse face were extracted from each recording and scored by blinded scorers. The scores were averaged at each time-point for each mouse cohort by the experimenters. von Frey testing of mice in their respective chambers immediately followed the video recordings. Withdrawal thresholds to probing of the hind-paws were determined before and after treatment administration. Paw withdrawal (PW) thresholds were determined by applying von Frey filaments to the plantar aspect of the hind-paws, and a withdrawal of the paw indicated a response. The withdrawal thresholds were then determined by the Dixon up-down method [10, 15] by blinded observers.

Thermal sensitivity was measured using the Hargreaves method [23]. Mice were placed on a heated glass floor (29°C) 20 minutes before each testing. Using a Hargreaves apparatus (IITC Model 390), a focused beam of high-intensity light was aimed at the plantar non-glabrous surface of the hind-paws. The intensity of the light was set to 30% of maximum with a cutoff value of 20 seconds. The latency to withdraw the hind paw was measured to the nearest 0.01 second. Baseline measures were obtained before treatment and at 1, 3, 5, 24, and 48 hours after administration.

Paw inflammation testing was carried out in a climate-controlled room (21 ± 2°C) by measuring the temperature of the animal's hind-paws. Animals were allowed to acclimate in the testing room for 1 hour preceding testing. Colorized infrared thermograms that captured the non-glabrous surface of the animal's hind-paws were obtained using a FLIR T-Series Thermal Imaging Camera. The thermograms were captured before experimental treatment and at 1, 3, 5, 24, and 48 hours after administration. Thermogram analysis was performed using the Windows-based PC application of the FLIR system. For each thermogram image, a straight line was drawn on the plantar surface of both hind-paws. The mean temperature was recorded from the average of each pixel along the drawn line. The raw temperatures were then plotted for ipsilateral and contralateral hind-paws for each animal.

Primary neuronal cultures

Male C57BL/6J or PAR3$^{-/-}$ mice were anesthetized with isoflurane and sacrificed by decapitation. Trigeminal or dorsal root ganglia (TGs or DRGs) were dissected into Hank's Balanced Salt Solution (HBSS), no calcium, no magnesium, on ice. Ganglia were digested in 1 mg/ml collagenase A (Roche) for 25 min at 37°C, followed by digestion in 1 mg/ml collagenase D and 30 U/ml papain (Worthington) for 20 min at 37°C. Ganglia were then triturated in 1 mg/ml trypsin inhibitor (Roche) and filtered through a 70 μm cell strainer (Corning). Cells were pelleted and resuspended in culture media, DMEM/F12 with GlutaMAX (Thermo Fisher Scientific) supplemented with 10% fetal bovine serum (FBS;

SH30088.03; Hyclone) and 1% penicillin/streptomycin (Pen-Strep; 15070–063; Gibco). Cells were plated 100 uL per dish onto pre-poly-D-lysine coated dishes (P35GC-1.5–10-C; MatTek) and allowed to adhere for 2 hours before being flooded with culture media with 10 ng/ml nerve growth factor (NGF; 01–125; Millipore). The plates were kept at 37°C and 5% CO_2 until use in calcium imaging.

Calcium Imaging

Ca^{2+} imaging was done using digital imaging microscopy. 48 hrs after plating, the cultures were washed with HBSS and loaded in 5 μM Fura2-AM (108964–32-5; Life Technologies) in HBSS for 45 min. Fura2 fluorescence was observed on an Olympus IX70 microscope (Waltham, MA, USA) with a 40× oil immersion objective after alternating excitation between 340 and 380 nm by a 75 W Xenon lamp linked to a Delta Ram V illuminator (PTI, London, Ontario, Canada) and a gel optic line. Images were captured using a high-speed camera using Olympus software. Ca^{2+} signaling response for each cell in the field of view was calculated from captured images by the ratio of 340nm/380nm. A cell was considered to respond to a stimulus when there was a 10% increase in the 340nm/380nm ratio. A minimum of one ratio per 2 seconds was calculated for all experiments.

All solutions were adjusted to pH 7.4 with NaCl or N-methyl-glucamine and osmolarity to 300 ± 5 mOsm with sucrose or ddH_2O apriori. Normal bath solution was applied to record a stable baseline, followed by compounds at 1 uM or 100 nM in phenol-free media, a washout in normal bath solution, and positive control with 50 mM KCl to identify neurons. Only cells responding to 50 mM KCl were considered for neuronal analysis. Normal bath solution consisted of NaCl (135 mM), KCl (5 mM), HEPES (10 mM), $CaCl_2$ (2 μM), $MgCl_2$ (1 μM), and glucose (10 μM) in ddH_2O. KCl (50 mM) solution was made up of NaCl (90 mM), KCl (50 mM), HEPES (10 mM), $CaCl_2$ (2 μM), $MgCl_2$ (1 μM), and glucose (10 μM) in ddH_2O.

Spinal Cord slice preparation

Adult (5–7 weeks old) male C57BL/6 mice were anesthetized with urethane (1.5–2.0 g/kg, i.p.). The lumbosacral spinal cord was quickly removed and placed in ice-cold sucrose-based artificial cerebrospinal fluid (aCSF), which was saturated with 95% O_2 and 5% CO_2 and maintained at room temperature. After extraction and still under anesthesia, animals were sacrificed by decapitation. Transverse slices (300–400 μm) were prepared using a vibrating micro slicer (VT1200s Leica). The slices were incubated at 32°C for at least 30 min in regular aCSF (NaCl 126 mM, KCl 3 mM, $MgCl_2$ 1.3 mM, $CaCl_2$ 2.5 mM, $NaHCO_3$ 26 mM, NaH_2PO_4 1.25 mM, and glucose 11 mM) equilibrated with 95% O_2 and 5% CO_2.

Electrophysiological recording

The slice was placed in the recording chamber and was then completely submerged and superfused at a rate of 1.5–3 ml/min with aCSF, which was saturated with 95% O_2 and 5% CO_2 and maintained at room temperature. Lamina IIo neurons in lumbar segments were identified as a translucent band under a microscope (BX51WIF; Olympus) with light transmitted from below. Whole-cell voltage-clamp recordings were made from lamina IIo neurons by using patch-pipettes fabricated from thin-walled, fiber-filled capillaries. Patch-pipette solution used to record spontaneous excitatory postsynaptic currents (sEPSCs)

contained: K-gluconate 135 mM, KCl 5 mM, $CaCl_2$ 0.5 mM, $MgCl_2$ 2 mM, EGTA 5 mM, HEPES 5 mM, Mg-ATP 5 mM (pH 7.3 adjusted with KOH, 300 mOsm). The patch-pipettes had a resistance of 8–10 Ω. As previously described [62], sEPSCs recordings were made at a holding potential (V_H) of −70 mV in the presence of 10 μM picrotoxin and 2 μM strychnine. Miniature EPSCs (mEPSCs) were recorded in the presence of 10 μM picrotoxin, 2 μM strychnine, and 0.5 μM tetrodotoxin. Signals were acquired using an Axopatch 700B amplifier. The data were stored and analyzed with a personal computer using pCLAMP 10.3 software. sEPSC events were detected and analyzed using Mini Analysis Program ver. 6.0.3. Numerical data are given as the mean ± SEM. Statistical significance was determined as $P < 0.05$ using the Student's *t*-test. In all cases, *n* refers to the number of the neurons studied.

Bioinformatics

Read counts for each coding gene for 204 single-cell RNA-sequencing profiles of mouse DRG sensory neurons were obtained from Gene Express Omnibus deposit (accession number GSE63576) [40]. t-SNE based non-linear embedding and visualization of the single-cell data sets was performed using Seurat package 2.2.1 [8, 18, 27] (Fig. 1A)

Power analysis

We performed a power analysis using a one-sided, unpaired t-test to estimate the sample size required for behavioral assays. Given that the α, β, and effect size was 0.05, 0.20, and 5.7266, respectively, the sample size for each group was determined to be less than four. Considering this, we performed all subsequent studies with four mice in each group (WT and $PAR3^{-/-}$).

Data analysis

All data are presented as means ± SEM unless otherwise noted. Effect sizes were determined by subtracting behavior scores for each time point from baseline measures. Absolute values were summed up and plotted for each group. For all behavioral data, statistics were performed using a two-way analysis of variance (ANOVA) with Bonferroni's multiple comparisons to assess genotype and time differences and unpaired t-tests for effect size comparison (refer to Supplemental Table 1 - 4). Statistical analysis was done using Graph Pad Prism Version 8.4.2 except for the electrophysiology data in Fig. 3, which was analyzed with an earlier version (v6).

RESULTS

Expression of PAR3 in sensory neurons

Expression of PAR3 has been characterized in megakaryocytes [12], vascular [6, 53], and alveolar endothelial cells [42]. However, not much is known about PAR3 expression in peripheral sensory neurons. To this end, we re-assessed *F2rl2* mRNA expression in mouse DRG single-cell RNA Seq datasets that were generated by Li et al., 2016 [40]. Non-linear embedding and visualization (using t-distributed stochastic neighbor embedding or tSNE) of high-dimensional whole-transcriptome gene expression profiles of individual DRG neurons were performed. It was demonstrated that *F2rl2* mRNA is highly enriched in peptidergic (*Calca*) and non-peptidergic (*P2rx3*) sensory neurons (Fig. 1A). Expression of *F2rl2* was

also detected in neuronal subpopulations that express *Nppb*, *Mrgpa3*, *Mrgprd,* and *Mrgpx1*, all of which are gene markers for distinct populations of pruriceptors [20, 43, 44]. PAR3 mRNA was also identified in subpopulations of Trpv1-encoding nociceptors, which are crucial for thermal hyperalgesia. A discrete population of *F2rl2* mRNA-expressing sensory neurons was enriched with *F2rl1* (encoding PAR2), which we have recently shown to be crucial for mechanical and affective pain responses in mice [25]. Finally, populations of mouse DRG neurons expressing PAR1 (*F2r*), PAR2 (*F2rl1*), and PAR4 (*F2rl3*) were also found in these neurons.

To further extend our studies on PAR3 expression in peripheral sensory neurons, we conducted RNAscope *in situ* hybridization on mouse TG neurons by probing for *Trpv1*, *F2rl2*, and *Nefh* mRNAs (Fig. 1B). Consistent with the findings from mouse DRG single-cell RNA Seq datasets, *F2rl2* mRNA was identified in a majority of TG neurons, approximately 83.3% (Fig. 1C). Additionally, most *Trpv1* mRNA-expressing neurons (81.6%) co-expressed F2rl2 mRNA (Fig. 1D), thereby confirming the broad expression patterns of PAR3 in peripheral nociceptors.

Peptidomimetic compound C660 is a selective activator of PAR3

To date, there have been no agonist ligands described that reliably and selectively target PAR3 *in vitro* and *in vivo*. A possible reason is that the receptor does not signal autonomously and, instead, seems to act as an accessory receptor for the activation of other PARs [22]. The capability of known PAR3 peptide derivatives to activate other PARs further complicates this area. Despite these caveats, we used a synthetic tethered ligand (STL) approach to design selective peptide agonists of PAR3 and evaluated their efficacy *in vitro* using Real Time Cell Analyzer (RTCA) assays [17]. A series of lipid-tethered ligands were synthesized by systematic mapping of N-terminal protease-revealed tethered sequences (refer to peptide list in Supplemental Fig. S1) and applied to TG neurons at 1 μM to evaluate Ca^{2+} response (Supplemental Fig. S1). We used TG neurons because we can generate a larger number of coverslips from fewer animals using TG rather than DRG. C660 (TFRGAPPNSFEEF-pego3-Hdc) elicited the highest Ca^{2+} response at 1 μM when compared to its truncated analogs C661 (GAPPNSFEEF-pego3-Hdc), C662 (TFRGAP-pego3-Hdc), C663 (TFR-pego3-Hdc), C737 (FEEF-pego3-Hdc), and C742 (NSFEEF-pego3-Hdc). Negative control C728 (Ac-pego3-Hdc) and C729 (scrambled C660 peptide PGTEFNFARESFP-pego3-Hdc) were not active. These findings suggest that, in addition to requiring the full-length peptide sequence (TFRGAPPNSFEEF) for PAR3 receptor activation, the lipid moiety attached to the peptide in C660 through a trimeric pego linker was crucial for membrane targeting and receptor activation (Fig. 2A).

We then challenged mouse DRG neuronal cultures with 100 nM C660 and found that it elicited a Ca^{2+} response that was comparable to that of cultured TGs (Fig. 2B) in terms of the number of cells that responded to treatment. Minimal Ca^{2+} responses were observed in cultured DRG neurons from $PAR3^{-/-}$ mice suggesting that C660 has a specific action at PAR3, at least in the mouse DRG (Fig. 2C). In the RTCA assay, HEK293 cells not induced to express PAR3 did not show a response to C660 (Fig. 2D). However, in human PAR3-expressing HEK293 cells, C660 induced a physiological response with an EC_{50} of ~ 900 nM

(Fig. 2E–2F), again suggesting a specific action of C660 on PAR3. Having established that C660 can induce Ca^{2+} responses in TG and DRG neurons, we sought to test the compound in an independent preparation with a different dependent measure. Spinal cord slices contain intrinsic neurons of the spinal cord and presynaptic terminals of nociceptors from the DRG. In spinal cord slice electrophysiology, C660 increased the frequency, but not amplitude, of postsynaptic events in lamina IIo neurons at 10 μM (Fig. 3A–C). Tetrodotoxin (TTX) did not influence the effect of C660 on the increased frequency of synaptic events in lamina IIo neurons (Fig. 3D–F). Because the frequency of these synaptic events is determined by presynaptic neurotransmitter release and the amplitude is due to postsynaptic receptor density, this finding likely suggests that C660 acts on presynaptic PAR3 expressed by DRG neurons to induce neurotransmitter release onto lamina IIo neurons in the dorsal horn.

The involvement of PAR3 in modulating pain behaviors is not well understood due to the scarcity of pharmacological tools that specifically target PAR3 *in vivo*. Therefore, having confirmed the selectivity of C660 for PAR3 using *in vitro* assays, we proceeded to evaluate mechanical and affective pain responses *in vivo*. Mice were injected with 30 pmol of C660 (dosage was estimated from the EC_{50}) in the hind paw after recording baseline (BL) measures. von Frey and grimace tests were performed at 1, 3, 5, 24, and 48 hours post-injection. Consistent with our *in vitro* findings, C660 evoked prolonged mechanical hypersensitivity and hyperalgesic priming in wildtype (WT) mice (Fig. 4A–D). On the other hand, in $PAR3^{-/-}$ mice, C660 had little acute effect, and the magnitude of the hyperalgesic priming effect was greatly reduced in these mice (Fig. 4A–D). Facial grimacing following C660 injection was noted in WT mice, although changes were transient (Fig. 4B). We did not note any changes in heat sensitivity in either strain of mice in response to C660 (Supplementary Fig. S2A–D). This suggests that PAR3 activation causes prolonged mechanical hypersensitivity and an affective pain response that is relatively brief. Our results show that C660 is a specific agonist of PAR3 *in vitro* with efficacy and selectivity *in vivo*.

Knockout of PAR3 potentiates pain responses to other PAR agonists

Considering that PAR3 is widely regarded as a coreceptor for other PARs, much focus has been drawn to its interactions with other PARs. In endothelial cells, for example, PAR3 is thought to form constitutive heterodimers with PAR1 that favor distinct signaling pathways from PAR1/PAR1 homodimer signaling [42]. However, the nature of these interactions in nociceptors and the pain behaviors they might elicit as a consequence are not well understood. We surmised that a knockdown of the non-signaling receptor PAR3 would impact mechanical and affective pain responses to other selective PAR agonists. Interestingly, we observed that PAR1 agonists, thrombin (10 units, i.pl) and TFFLLR-NH_2 (100 μg, i.pl) induced mechanical hypersensitivity in both WT and $PAR3^{-/-}$, but these responses were significantly more robust and prolonged in $PAR3^{-/-}$ mice. Additionally, facial grimacing was noted in the $PAR3^{-/-}$ mice up to 5 hours post-injection with either thrombin or TFFLLR-NH_2 (Fig. 5A–B).

We next evaluated pain responses after injecting the PAR2 agonist, 2-aminothiazo-4-yl-LIGRL-NH_2 (2AT; 30 pmol) into the hind paw of WT and $PAR3^{-/-}$ mice. 2AT evoked mechanical hypersensitivity and facial grimacing in both WT and $PAR3^{-/-}$ mice without any

effect of genotype (Fig. 6A–B). We also assessed hyperalgesic priming in these mice because our previous work demonstrated that PAR2 activation is sufficient to induce priming [57]. Unexpectedly, when we challenged these mice with PGE_2 injection into the previously stimulated hind paw, we observed a profound deficit in priming in the $PAR3^{-/-}$ mice in the von Frey assay (Fig. 6C–D).

The mast cell degranulating compound 48/80 produces pain that is mediated, at least in part, by mast cell tryptase action on PAR2 [7]. We tested the effect of 48/80 injections into the paw in WT and $PAR3^{-/-}$ mice (Supplementary Fig. S3A–B). The effect of 48/80 on mechanical hypersensitivity was blunted in $PAR3^{-/-}$ mice compared to WT mice, and there was little grimacing effect observed in this experiment. Therefore, PAR3 does not seem to regulate PAR2-mediated pain responses in response to direct agonist stimulation of the receptor in the DRG regions, but there appears to be a contribution of PAR3 to hyperalgesic priming. PAR3 may play a more significant role in pain responses when endogenous proteases activate PAR2. Intraplantar administration of the PAR4 agonist peptide AYPGKF-NH_2 (100 μg) did not significantly change withdrawal thresholds and grimacing in WT while a transient effect was seen in $PAR3^{-/-}$ mice (Fig. 7A–B).

Hyperalgesic priming deficits in PAR3 knockout mice

Hyperalgesic priming is a two-hit model where exposure to a first stimulus causes a second, normally non-noxious stimulus to cause a long-lasting pain state [2, 29, 49]. The underlying mechanisms of hyperalgesic priming involve plasticity in nociceptors [34, 46, 50, 52]. As shown in Fig. 6, we observed a profound deficit in hyperalgesic priming in $PAR3^{-/-}$ mice exposed to a PAR2 specific agonist. A potential explanation for this is a loss of PGE_2 response in $PAR3^{-/-}$ mice. We tested this directly by exposing mice to a high dose of PGE_2 (10 μg). This dose of PGE_2 caused robust mechanical hypersensitivity and grimacing in WT and $PAR3^{-/-}$ mice (Supplementary Fig. S4A–B). When these mice were challenged with 100 ng PGE_2, the animals of both genotypes displayed a response consistent with the development of hyperalgesic priming (Supplementary Fig. S4C–D). This shows that $PAR3^{-/-}$ mice respond to PGE_2, and these mice can display hyperalgesic priming, but this depends on the first hit stimulus.

To further explore which types of stimuli might show deficits in hyperalgesic priming in $PAR3^{-/-}$ mice, we assessed various other priming factors. The inflammatory cytokine interleukin 6 (IL-6) produced similar acute responses in both genotypes (Fig. 8A–B), but hyperalgesic priming was diminished as measured by mechanical hypersensitivity and grimacing in $PAR3^{-/-}$ mice (Fig. 8C–D). Using carrageenan as the priming stimulus, male WT and $PAR3^{-/-}$ mice responded similarly to the inflammagen acutely (Supplementary Fig. S5A–B), but the hyperalgesic priming was again reduced in the $PAR3^{-/-}$ mice (Supplementary Fig. S5C–D). Similar results were obtained in female mice (Supplementary Fig. S6A–D). These experiments suggest that hyperalgesic priming mechanisms in response to some, but not all, priming stimuli are impaired in the absence of PAR3.

DISCUSSION

Our work begins to define a role of PAR3 in nociception. PAR3 is widely distributed in mouse sensory neurons and may be crucial for inducing nociceptor hyperexcitability and mechanical hyperalgesia. We noted that PAR3 mRNA expression is detected in a majority of nociceptors regardless of the peptidergic and non-peptidergic nature of these neuronal subtypes. PAR3 expression overlaps with the presence of PAR1 or PAR2 in discrete neuronal subpopulations, likely suggesting its role in modulating PAR1- and PAR2-driven pain behaviors. We tested this hypothesis *in vivo* and observed that the involvement of PAR1 and PAR2 agonists in evoking pain stimuli are potentiated in the absence of PAR3. Critically, we have developed a novel lipid tethered peptidomimetic agonist for PAR3, C660, and demonstrated its activity and specificity both *in vitro* and *in vivo*. This tool will be useful for further understanding the role of PAR3 in pain and other areas. A remarkable phenotype of the $PAR3^{-/-}$ mice is the loss of hyperalgesic priming in response to IL-6, carrageenan, and PAR2 agonist 2AT, suggesting that PAR3 has a role in the plasticity of afferent neurons. These primary conclusions emerging from our experiments are discussed further below.

PAR3 expression has been well characterized in human and murine platelets [30, 31, 55], vascular smooth muscle cells [6], endothelial cells [14, 33, 55], and monocytes [12], yet its presence and function in sensory neurons have not been thoroughly investigated. A previous histological study by Zhu et al. 2005 showed that, in rat DRG, PAR3 mRNA was the highest expressed of all PARs and was detected in at least 40% of neurons. In that study, they found that 80% of these PAR3 expressing cells also co-expressed CGRP [66]. Our analysis of previously published mouse single-cell RNA seq findings confirm the broad distribution patterns of PAR3 mRNA in DRG neurons and show that the mRNA is expressed in both peptidergic and non-peptidergic mouse afferents. We independently corroborated this expression pattern in mouse TG using RNAscope. Chamessian and colleagues showed that PAR3 mRNA is expressed in dorsal horn somatostatin-positive interneurons, which are known to modulate mechanical pain [9, 45]. While we cannot confirm that we recorded from somatostatin-positive neurons in lamina IIo, our spinal cord slice experiments showed an apparent presynaptic effect of PAR3 activation, suggesting that PAR3 expression in primary afferents can regulate neurotransmitter release onto dorsal horn neurons. Our Ca^{2+} imaging experiments on mouse DRG and TG neurons confirm that PAR3 is functionally active in at least a subset of sensory neurons. A larger population of DRG neurons expressed PAR3 mRNA than were activated by C660. This may be explained by receptor hetero-oligomerization with an unknown receptor pair or by unexplained aspects of C660 pharmacology at natively expressed PAR3. Given that we observed enhanced behavioral responses with a PAR1 agonist in PAR3 KO mice, we favor the idea that PAR1/PAR3 heteromers confer Ca^{2+} signaling in sensory neurons. Our experiments in HEK293 cells, which natively express PAR1 [37], support the conclusion that expressing PAR3 is sufficient to confer Ca^{2+} signaling in cells exposed to C660. Another possibility is that PAR3 is downregulated in cultured neurons. Our work using RNA sequencing on mouse DRG neurons supports this possibility as well, at least at the RNA level [63]. Both explanations await further experimental confirmation.

PAR homo- and hetero-oligomerization interactions have garnered considerable interest over the years, with several studies documenting the colocalization and transactivation of these GPCRs in different physiological settings. For instance, PAR3 associates with PAR1 in endothelial cells to potentiate the responsiveness of PAR1 to thrombin [42]. In other cases, PAR3 expression has been shown to counteract PAR1 signaling [64]. Our results support the conclusion that PAR3 suppresses PAR1 signaling in sensory neurons. PAR1 agonists caused much larger pain responses when measured with mechanical hypersensitivity and grimacing in mice lacking PAR3. PAR2 plays a critical role in many types of persistent pain [24, 25, 32, 38, 58, 65]. The specific PAR2 agonist 2AT did not show any differences in acute responses in $PAR3^{-/-}$ mice, but there was a small decrease in response to the mast cell degranulator 48/80 in these mice. Our findings suggest that PAR3 may not be involved in regulating PAR2 activity regardless of receptor activation method. PAR3 can also complex with PAR4 in mouse platelets to facilitate the cleavage and activation of PAR4 at low thrombin concentrations [47]. However, another study found that PAR3 acts as a break on PAR4 signaling in platelets [3], similar to what has been described for PAR3 with PAR1 and PAR2. Nevertheless, we noted only very transient PAR4-mediated pain behaviors in WT or $PAR3^{-/-}$ mice, suggesting that PAR4 does not play an active role, or only a very minor one, in nociception from the paw. This may be different from nociception from visceral organs where PAR4 has been shown to play an important role [5, 36, 61]. Although it is commonly thought that PAR3 cooperates with other PARs to initiate downstream signaling cascades, there is also evidence that activated PAR3 may signal autonomously to stimulate calcium mobilization and ERK1/2 phosphorylation [6, 48]. Single-cell sequencing data [40] suggests that PAR3 is expressed in some nociceptor subtypes that do not express PAR1, −2, or −4. Therefore, we cannot exclude the possibility that PAR3 may be signaling without cooperating with other PARs in certain neuronal subpopulations. The functional role of PAR3 in those sensory neuron subtypes will need to be characterized with conditional knockout technologies.

While the oligomerization of PARs in different cell types contributes to increased receptor diversity and function, it also poses a challenge in developing agonists and antagonists that selectively act on PARs, including PAR3. To date, there are no known PAR3 antagonists, and existing agonists lack potency and efficacy and have been shown to activate other PARs [1, 22, 41, 54, 59]. Using the synthetic tethered ligand approach, we have developed a more selective agonist, C660, by lipidating the peptide sequence to mimic membrane tethering that occurs with PAR endogenous ligands [17]. We show that C660 evokes Ca^{2+} responses in DRG and TG neurons and physiological responses in human PAR3-expressing cells with an EC_{50} of approximately 900 nM. Notably, both of these responses are absent when PAR3 is not expressed. However, most DRG and TG neurons expressed PAR3, but only a subset of them showed measurable Ca^{2+} responses when C660 was applied to these cultures. We do not currently understand if PAR3 expression alone is sufficient for signaling in response to C660, although it appears to be necessary. Our *in vivo* experiments further validate the use of C660 as a pharmacological agonist of PAR3. C660 induced mechanical hypersensitivity and caused hyperalgesic priming in WT mice, but these effects were absent in PAR3 deficient mice, again supporting the specificity of this new PAR3 agonist. We anticipate that

C660 will be a useful tool for further understanding the physiological role of PAR3 in different contexts and species.

Hyperalgesic priming is an animal model system used to better understand the mechanisms of nociceptor plasticity that may be involved in chronic pain [34, 50]. Experimental models for hyperalgesic priming are based on the concept that the initial application of noxious stimuli may subsequently elicit prolonged pain responses to an ordinarily non-noxious stimulus [52]. In our experiments, we “primed” with various stimuli, including C660, 2AT, IL-6, or carrageenan, allowing animals to completely recover from the initial stimulus before applying the second “hit”. PAR3 activation with C660 caused hyperalgesic priming in mice suggesting that PAR3 activation is sufficient to induce a primed state. Interestingly, in mice lacking PAR3, hyperalgesic priming failed to develop in response to most of these stimuli. This loss of hyperalgesic priming occurred in both male and female mice, at least in the carrageenan model. We acknowledge that we did not test for sex effects in most experiments, which is a shortcoming of our work. The deficit in hyperalgesic priming we observed cannot be explained by a loss of PGE_2 sensitivity because $PAR3^{-/-}$ mice responded to a high dose PGE_2 injection and even showed priming to this stimulus. While we do not have a mechanistic explanation for why PAR3 appears to play a crucial role in nociceptor plasticity in some contexts and not in others, further investigations along these lines may reveal aspects of PAR3 signaling in nociceptors that make the receptor a drug target for chronic pain.

Supplementary Material

Refer to Web version on PubMed Central for supplementary material.

Acknowledgments

Disclosures: The authors declare no conflicts of interest. This work was supported by NIH grants NS098826 (TJP, GD, SB, and JV), NS065926 (TJP), NS072204 (GD), and training grant NS096963 (SNH).

REFERENCES

1. Alexander SPH, Christopoulos A, Davenport AP, Kelly E, Mathie A, Peters JA, Veale EL, Armstrong JF, Faccenda E, Harding SD, Pawson AJ, Sharman JL, Southan C, Davies JA, Collaborators C: THE CONCISE GUIDE TO PHARMACOLOGY 2019/20: G protein-coupled receptors. Br J Pharmacol 176 Suppl 1:S21–S141, 2019. [PubMed: 31710717]
2. Aley KO, Messing RO, Mochly-Rosen D, Levine JD: Chronic hypersensitivity for inflammatory nociceptor sensitization mediated by the epsilon isozyme of protein kinase C. J Neurosci 20:4680–5, 2000. [PubMed: 10844037]
3. Arachiche A, de la Fuente M, Nieman MT: Calcium mobilization and protein kinase C activation downstream of protease activated receptor 4 (PAR4) is negatively regulated by PAR3 in mouse platelets. PLoS One 8:e55740, 2013. [PubMed: 23405206]
4. Boitano S, Flynn AN, Schulz SM, Hoffman J, Price TJ, Vagner J: Potent agonists of the protease activated receptor 2 (PAR2). J Med Chem 54:1308–13, 2011. [PubMed: 21294569]
5. Bradesi S: PAR4: a new role in the modulation of visceral nociception. Neurogastroenterology and motility : the official journal of the European Gastrointestinal Motility Society 21:1129–32, 2009. [PubMed: 19804483]

6. Bretschneider E, Spanbroek R, Lotzer K, Habenicht AJ, Schror K: Evidence for functionally active protease-activated receptor-3 (PAR-3) in human vascular smooth muscle cells. Thromb Haemost 90:704–9, 2003. [PubMed: 14515192]
7. Bunnett NW: Protease-activated receptors: how proteases signal to cells to cause inflammation and pain. Semin Thromb Hemost 32 Suppl 1:39–48, 2006.
8. Butler A, Hoffman P, Smibert P, Papalexi E, Satija R: Integrating single-cell transcriptomic data across different conditions, technologies, and species. Nature biotechnology 36:411–20, 2018.
9. Chamessian A, Young M, Qadri Y, Berta T, Ji RR, Van de Ven T: Transcriptional Profiling of Somatostatin Interneurons in the Spinal Dorsal Horn. Sci Rep 8:6809, 2018. [PubMed: 29717160]
10. Chaplan SR, Bach FW, Pogrel JW, Chung JM, Yaksh TL: Quantitative assessment of tactile allodynia in the rat paw. J Neurosci Methods 53:55–63, 1994. [PubMed: 7990513]
11. Cocks TM, Moffatt JD: Protease-activated receptors: sentries for inflammation? Trends Pharmacol Sci 21:103–8, 2000. [PubMed: 10689364]
12. Colognato R, Slupsky JR, Jendrach M, Burysek L, Syrovets T, Simmet T: Differential expression and regulation of protease-activated receptors in human peripheral monocytes and monocyte-derived antigen-presenting cells. Blood 102:2645–52, 2003. [PubMed: 12805069]
13. Coughlin SR: Thrombin signalling and protease-activated receptors. Nature 407:258–64, 2000. [PubMed: 11001069]
14. Cupit LD, Schmidt VA, Bahou WF: Proteolytically activated receptor-3. A member of an emerging gene family of protease receptors expressed on vascular endothelial cells and platelets. Trends Cardiovasc Med 9:42–8, 1999. [PubMed: 10189966]
15. Dixon WJ: Efficient analysis of experimental observations. Annu Rev Pharmacol Toxicol 20:441–62, 1980. [PubMed: 7387124]
16. Flynn AN, Tillu DV, Asiedu MN, Hoffman J, Vagner J, Price TJ, Boitano S: The protease-activated receptor-2-specific agonists 2-aminothiazol-4-yl-LIGRL-NH2 and 6-aminonicotinyl-LIGRL-NH2 stimulate multiple signaling pathways to induce physiological responses in vitro and in vivo. J Biol Chem 286:19076–88, 2011. [PubMed: 21467041]
17. Flynn AN, Hoffman J, Tillu DV, Sherwood CL, Zhang Z, Patek R, Asiedu MN, Vagner J, Price TJ, Boitano S: Development of highly potent protease-activated receptor 2 agonists via synthetic lipid tethering. FASEB J 27:1498–510, 2013. [PubMed: 23292071]
18. Gribov A, Sill M, Luck S, Rucker F, Dohner K, Bullinger L, Benner A, Unwin A: SEURAT: visual analytics for the integrated analysis of microarray data. BMC Med Genomics 3:21, 2010. [PubMed: 20525257]
19. Hamilton JR, Trejo J: Challenges and Opportunities in Protease-Activated Receptor Drug Development. Annu Rev Pharmacol Toxicol 57:349–73, 2017. [PubMed: 27618736]
20. Han L, Ma C, Liu Q, Weng HJ, Cui Y, Tang Z, Kim Y, Nie H, Qu L, Patel KN, Li Z, McNeil B, He S, Guan Y, Xiao B, Lamotte RH, Dong X: A subpopulation of nociceptors specifically linked to itch. Nat Neurosci 16:174–82, 2013. [PubMed: 23263443]
21. Han X, Hofmann L, de la Fuente M, Alexander N, Palczewski K, Consortium I, Nieman MT: PAR4 activation involves extracellular loop 3 and transmembrane residue Thr153. Blood 136:2217–28, 2020. [PubMed: 32575122]
22. Hansen KK, Saifeddine M, Hollenberg MD: Tethered ligand-derived peptides of proteinase-activated receptor 3 (PAR3) activate PAR1 and PAR2 in Jurkat T cells. Immunology 112:183–90, 2004. [PubMed: 15147561]
23. Hargreaves K, Dubner R, Brown F, Flores C, Joris J: A new and sensitive method for measuring thermal nociception in cutaneous hyperalgesia. Pain 32:77–88, 1988. [PubMed: 3340425]
24. Hassler SN, Ahmad FB, Burgos-Vega CC, Boitano S, Vagner J, Price TJ, Dussor G: Protease activated receptor 2 (PAR2) activation causes migraine-like pain behaviors in mice. Cephalalgia:333102418779548, 2018.
25. Hassler SN, Kume M, Mwirigi J, Ahmad A, Shiers S, Wangzhou A, Ray P, Belugin SN, Naik DK, Burton MD, Vagner J, Boitano S, Akopian AN, Dussor G, Price TJ: The cellular basis of protease activated receptor type 2 (PAR2) evoked mechanical and affective pain. JCI Insight, 2020.

26. Heuberger DM, Schuepbach RA: Protease-activated receptors (PARs): mechanisms of action and potential therapeutic modulators in PAR-driven inflammatory diseases. Thromb J 17:4, 2019. [PubMed: 30976204]
27. Hockley JRF, Taylor TS, Callejo G, Wilbrey AL, Gutteridge A, Bach K, Winchester WJ, Bulmer DC, McMurray G, Smith ESJ: Single-cell RNAseq reveals seven classes of colonic sensory neuron. Gut 68:633–44, 2019. [PubMed: 29483303]
28. Hollenberg MD, Mihara K, Polley D, Suen JY, Han A, Fairlie DP, Ramachandran R: Biased signalling and proteinase-activated receptors (PARs): targeting inflammatory disease. Br J Pharmacol 171:1180–94, 2014. [PubMed: 24354792]
29. Hucho T, Levine JD: Signaling pathways in sensitization: toward a nociceptor cell biology. Neuron 55:365–76, 2007. [PubMed: 17678851]
30. Ishihara H, Connolly AJ, Zeng D, Kahn ML, Zheng YW, Timmons C, Tram T, Coughlin SR: Protease-activated receptor 3 is a second thrombin receptor in humans. Nature 386:502–6, 1997. [PubMed: 9087410]
31. Ishihara H, Zeng D, Connolly AJ, Tam C, Coughlin SR: Antibodies to protease-activated receptor 3 inhibit activation of mouse platelets by thrombin. Blood 91:4152–7, 1998. [PubMed: 9596661]
32. Jimenez-Vargas NN, Pattison LA, Zhao P, Lieu T, Latorre R, Jensen DD, Castro J, Aurelio L, Le GT, Flynn B, Herenbrink CK, Yeatman HR, Edgington-Mitchell L, Porter CJH, Halls ML, Canals M, Veldhuis NA, Poole DP, McLean P, Hicks GA, Scheff N, Chen E, Bhattacharya A, Schmidt BL, Brierley SM, Vanner SJ, Bunnett NW: Protease-activated receptor-2 in endosomes signals persistent pain of irritable bowel syndrome. Proc Natl Acad Sci U S A 115:E7438–E47, 2018. [PubMed: 30012612]
33. Kalashnyk O, Petrova Y, Lykhmus O, Mikhalovska L, Mikhalovsky S, Zhukova A, Gnatenko D, Bahou W, Komisarenko S, Skok M: Expression, function and cooperating partners of protease-activated receptor type 3 in vascular endothelial cells and B lymphocytes studied with specific monoclonal antibody. Mol Immunol 54:319–26, 2013. [PubMed: 23352962]
34. Kandasamy R, Price TJ: The pharmacology of nociceptor priming. Handb Exp Pharmacol 227:15–37, 2015. [PubMed: 25846612]
35. Kaufmann R, Schulze B, Krause G, Mayr LM, Settmacher U, Henklein P: Proteinase-activated receptors (PARs)--the PAR3 Neo-N-terminal peptide TFRGAP interacts with PAR1. Regul Pept 125:61–6, 2005. [PubMed: 15582715]
36. Kouzoukas DE, Ma F, Meyer-Siegler KL, Westlund KN, Hunt DE, Vera PL: Protease-Activated Receptor 4 Induces Bladder Pain through High Mobility Group Box-1. PLoS One 11:e0152055, 2016. [PubMed: 27010488]
37. Lachmann A, Torre D, Keenan AB, Jagodnik KM, Lee HJ, Wang L, Silverstein MC, Ma'ayan A: Massive mining of publicly available RNA-seq data from human and mouse. Nat Commun 9:1366, 2018. [PubMed: 29636450]
38. Lam DK, Schmidt BL: Serine proteases and protease-activated receptor 2-dependent allodynia: a novel cancer pain pathway. Pain 149:263–72, 2010. [PubMed: 20189717]
39. Langford DJ, Bailey AL, Chanda ML, Clarke SE, Drummond TE, Echols S, Glick S, Ingrao J, Klassen-Ross T, Lacroix-Fralish ML, Matsumiya L, Sorge RE, Sotocinal SG, Tabaka JM, Wong D, van den Maagdenberg AM, Ferrari MD, Craig KD, Mogil JS: Coding of facial expressions of pain in the laboratory mouse. Nature methods 7:447–9, 2010. [PubMed: 20453868]
40. Li CL, Li KC, Wu D, Chen Y, Luo H, Zhao JR, Wang SS, Sun MM, Lu YJ, Zhong YQ, Hu XY, Hou R, Zhou BB, Bao L, Xiao HS, Zhang X: Somatosensory neuron types identified by high-coverage single-cell RNA-sequencing and functional heterogeneity. Cell research 26:83–102, 2016. [PubMed: 26691752]
41. Macfarlane SR, Seatter MJ, Kanke T, Hunter GD, Plevin R: Proteinase-activated receptors. Pharmacol Rev 53:245–82, 2001. [PubMed: 11356985]
42. McLaughlin JN, Patterson MM, Malik AB: Protease-activated receptor-3 (PAR3) regulates PAR1 signaling by receptor dimerization. Proc Natl Acad Sci U S A 104:5662–7, 2007. [PubMed: 17376866]
43. Meixiong J, Dong X: Mas-Related G Protein-Coupled Receptors and the Biology of Itch Sensation. Annu Rev Genet 51:103–21, 2017. [PubMed: 29178819]

44. Mishra SK, Hoon MA: The cells and circuitry for itch responses in mice. Science 340:968–71, 2013. [PubMed: 23704570]
45. Moehring F, Halder P, Seal RP, Stucky CL: Uncovering the Cells and Circuits of Touch in Normal and Pathological Settings. Neuron 100:349–60, 2018. [PubMed: 30359601]
46. Moy JK, Khoutorsky A, Asiedu MN, Black BJ, Kuhn JL, Barragan-Iglesias P, Megat S, Burton MD, Burgos-Vega CC, Melemedjian OK, Boitano S, Vagner J, Gkogkas CG, Pancrazio JJ, Mogil JS, Dussor G, Sonenberg N, Price TJ: The MNK-eIF4E Signaling Axis Contributes to Injury-Induced Nociceptive Plasticity and the Development of Chronic Pain. J Neurosci 37:7481–99, 2017. [PubMed: 28674170]
47. Nakanishi-Matsui M, Zheng YW, Sulciner DJ, Weiss EJ, Ludeman MJ, Coughlin SR: PAR3 is a cofactor for PAR4 activation by thrombin. Nature 404:609–13, 2000. [PubMed: 10766244]
48. Ostrowska E, Reiser G: The protease-activated receptor-3 (PAR-3) can signal autonomously to induce interleukin-8 release. Cell Mol Life Sci 65:970–81, 2008. [PubMed: 18264801]
49. Parada CA, Reichling DB, Levine JD: Chronic hyperalgesic priming in the rat involves a novel interaction between cAMP and PKCepsilon second messenger pathways. Pain 113:185–90, 2005. [PubMed: 15621379]
50. Price TJ, Inyang KE: Commonalities between pain and memory mechanisms and their meaning for understanding chronic pain. Prog Mol Biol Transl Sci 131:409–34, 2015. [PubMed: 25744681]
51. Ramachandran R, Hollenberg MD: Proteinases and signalling: pathophysiological and therapeutic implications via PARs and more. Br J Pharmacol 153 Suppl 1:S263–82, 2008. [PubMed: 18059329]
52. Reichling DB, Levine JD: Critical role of nociceptor plasticity in chronic pain. Trends Neurosci 32:611–8, 2009. [PubMed: 19781793]
53. Rosenkranz AC, Rauch BH, Doller A, Eberhardt W, Bohm A, Bretschneider E, Schror K: Regulation of human vascular protease-activated receptor-3 through mRNA stabilization and the transcription factor nuclear factor of activated T cells (NFAT). Mol Pharmacol 80:337–44, 2011. [PubMed: 21596928]
54. Russell FA, McDougall JJ: Proteinase activated receptor (PAR) involvement in mediating arthritis pain and inflammation. Inflamm Res 58:119–26, 2009. [PubMed: 19184346]
55. Schmidt VA, Nierman WC, Maglott DR, Cupit LD, Moskowitz KA, Wainer JA, Bahou WF: The human proteinase-activated receptor-3 (PAR-3) gene. Identification within a Par gene cluster and characterization in vascular endothelial cells and platelets. J Biol Chem 273:15061–8, 1998. [PubMed: 9614115]
56. Steinhoff M, Buddenkotte J, Shpacovitch V, Rattenholl A, Moormann C, Vergnolle N, Luger TA, Hollenberg MD: Proteinase-activated receptors: transducers of proteinase-mediated signaling in inflammation and immune response. Endocr Rev 26:1–43, 2005. [PubMed: 15689571]
57. Tillu DV, Hassler SN, Burgos-Vega CC, Quinn TL, Sorge RE, Dussor G, Boitano S, Vagner J, Price TJ: Protease-activated receptor 2 activation is sufficient to induce the transition to a chronic pain state. Pain 156:859–67, 2015. [PubMed: 25734998]
58. Vergnolle N, Bunnett NW, Sharkey KA, Brussee V, Compton SJ, Grady EF, Cirino G, Gerard N, Basbaum AI, Andrade-Gordon P, Hollenberg MD, Wallace JL: Proteinase-activated receptor-2 and hyperalgesia: A novel pain pathway. Nat Med 7:821–6, 2001. [PubMed: 11433347]
59. Vergnolle N: Protease-activated receptors as drug targets in inflammation and pain. Pharmacol Ther 123:292–309, 2009. [PubMed: 19481569]
60. Wang H, Ubl JJ, Reiser G: Four subtypes of protease-activated receptors, co-expressed in rat astrocytes, evoke different physiological signaling. Glia 37:53–63, 2002. [PubMed: 11746783]
61. Wang W, Bo Q, Du J, Yu X, Zhu K, Cui J, Zhao H, Wang Y, Shi B, Zhu Y: Endogenous H2S sensitizes PAR4-induced bladder pain. Am J Physiol Renal Physiol 314:F1077–F86, 2018. [PubMed: 29357418]
62. Wang Z, Jiang C, He Q, Matsuda M, Han Q, Wang K, Bang S, Ding H, Ko MC, Ji RR: Anti-PD-1 treatment impairs opioid antinociception in rodents and nonhuman primates. Sci Transl Med 12, 2020.
63. Wangzhou A, McIlvried LA, Paige C, Barragan-Iglesias P, Shiers S, Ahmad A, Guzman CA, Dussor G, Ray PR, Gereau RWt, Price TJ: Pharmacological target-focused transcriptomic analysis

of native vs cultured human and mouse dorsal root ganglia. Pain 161:1497–517, 2020. [PubMed: 32197039]

64. Wysoczynski M, Liu R, Kucia M, Drukala J, Ratajczak MZ: Thrombin regulates the metastatic potential of human rhabdomyosarcoma cells: distinct role of PAR1 and PAR3 signaling. Mol Cancer Res 8:677–90, 2010. [PubMed: 20442298]
65. Zhao P, Lieu T, Barlow N, Sostegni S, Haerteis S, Korbmacher C, Liedtke W, Jimenez-Vargas NN, Vanner SJ, Bunnett NW: Neutrophil Elastase Activates Protease-activated Receptor-2 (PAR2) and Transient Receptor Potential Vanilloid 4 (TRPV4) to Cause Inflammation and Pain. J Biol Chem 290:13875–87, 2015. [PubMed: 25878251]
66. Zhu WJ, Yamanaka H, Obata K, Dai Y, Kobayashi K, Kozai T, Tokunaga A, Noguchi K: Expression of mRNA for four subtypes of the proteinase-activated receptor in rat dorsal root ganglia. Brain Res 1041:205–11, 2005. [PubMed: 15829229]

Highlights

- PAR3 is broadly distributed in mouse DRGs and is co-expressed with other PARs.
- Novel peptidomimetic compound C660 selectively activates PAR3.
- Knocking out PAR3 potentiates the pronociceptive effects of PAR1 agonists.
- PAR3 plays a crucial role in hyperalgesic priming.

Perspective

We evaluated the role of PAR3, a G-protein coupled receptor, in nociception by developing a selective peptide agonist. Our findings suggest that PAR3 contributes to nociception in various contexts and plays a role in modulating the activity of other PARs.

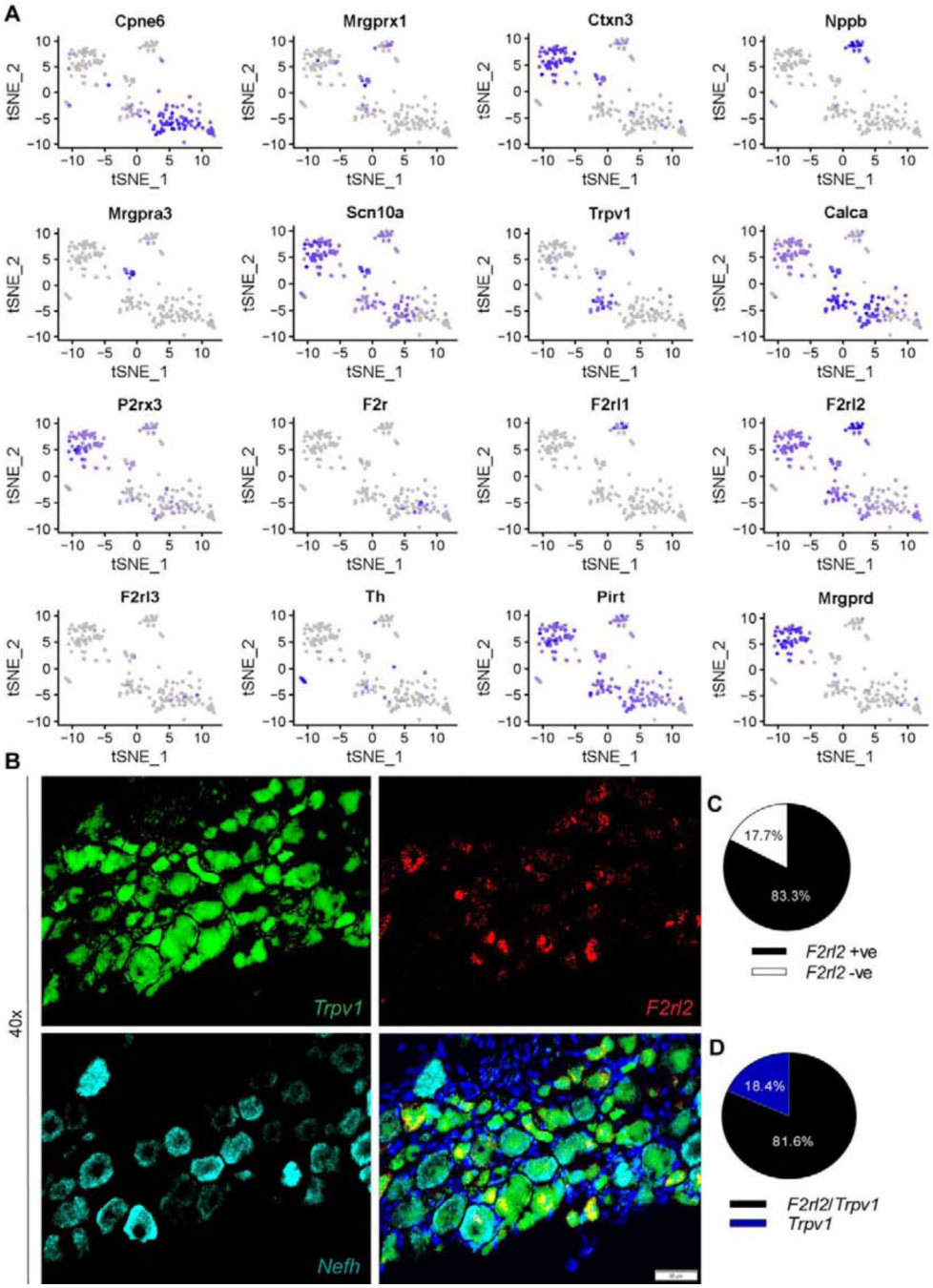

Figure 1. *F2rl2 mRNA* is expressed across sensory neuron populations.

(A) t-SNE based visualization (using Seurat) of single-cell datasets demonstrate that *F2rl2* mRNA is expressed in a majority of DRG sensory neuron subtypes. *F2rl2* mRNA was detected in populations of sensory neurons co-expressing either *F2r* and *F2rl1* mRNAs that encode PAR1 and PAR2, respectively. Little to no overlap was observed between *F2rl2* and *F2rl3* (encoding PAR4) expressing sensory populations. Of note, *F2rl2* mRNA appears to be broadly distributed among the peptidergic and non-peptidergic subpopulations of sensory neurons, as well as in *Trpv1*+ neurons. A proportion of neurons expressing itch markers

Nppb, *Mrgprx1*, *Mrgpra3, and Mrgprd* co-expressed *F2rl2 mRNA*. Gene titles are indicated at the top of each t-SNE plot. Color saturation denotes normalized gene expression levels. (B) Representative 40X images of mouse TG neurons labeled with RNAscope *in situ* hybridization for *Trpv1* (green), *F2rl2* (red), and *Nefh* (cyan) mRNAs, and DAPI (blue). Scale bar: 50 μm. Pie charts illustrate that (C) F2rl2 mRNA is present in a majority of TG neurons (83.3% ± 1.54) and (D) colocalizes with most Trpv1 mRNA expressing neurons (81.6% ± 2.86) (n = 4).

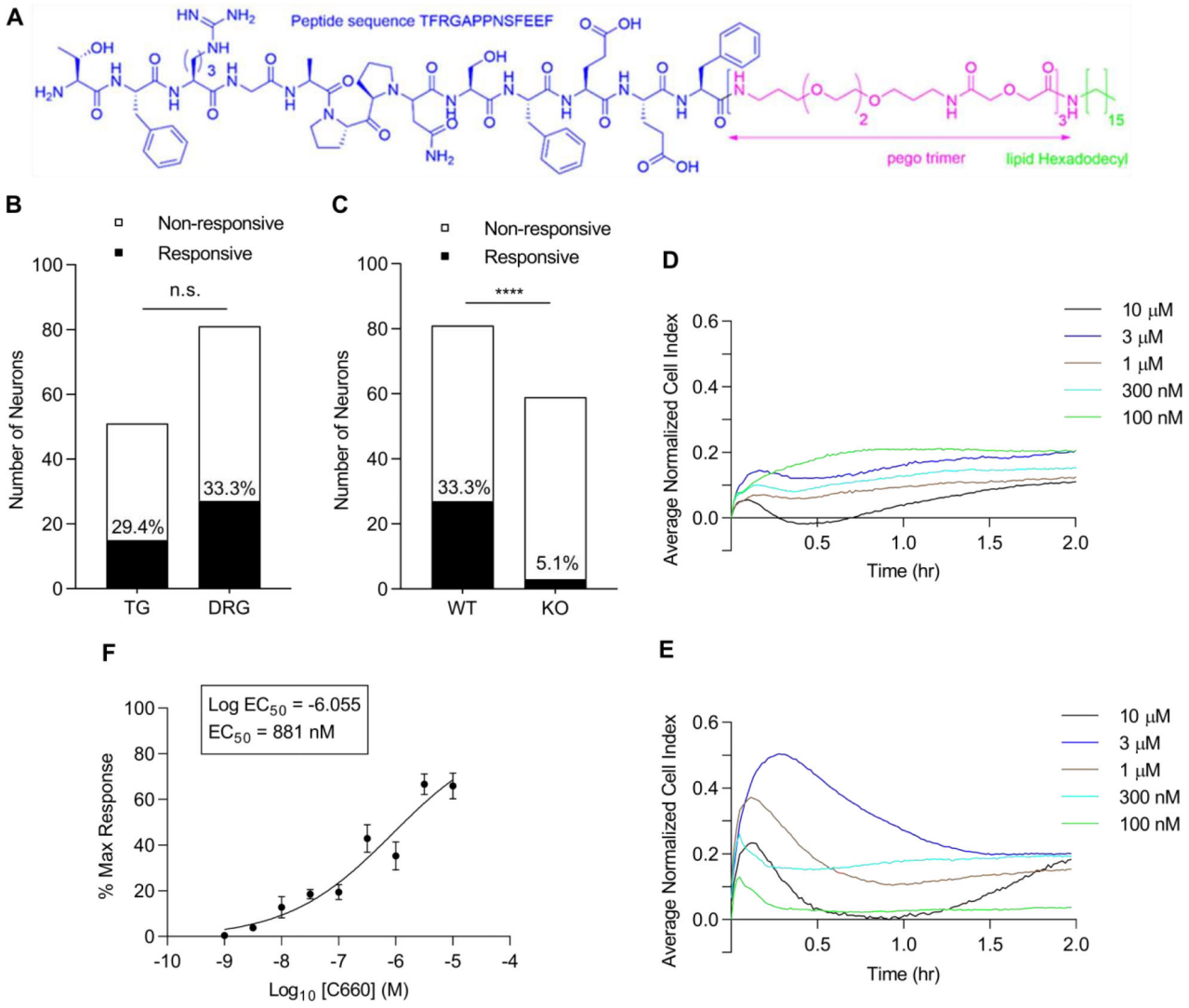

Figure 2. Peptidomimetic agonist C660 elicits responses specific to PAR3-expressing cells.

(A) Full-length structure of compound C660. The canonical structure of the human PAR3 receptor ligand (Thr39-Phe51), denoted in blue, is tethered to a short polyethylene glycol linker, pego3 (pink), and a lipid moiety (green). (Panel B and C) WT and PAR3$^{-/-}$ TG or DRG cultures were treated with PAR3 agonist peptide, C660 (100nM), after which the neuronal responses were evaluated based on a 10% ratiometric increase in 340nm/380nm. Only cells with a response to KCl (50 mM) were considered for analysis. Responses in calcium imaging are shown as contingency graphs. (B) The Ca^{2+} responses elicited by C660 (100 nM) in cultured TG (29.4%) and DRG (33.3%) neurons are comparable (n = 51 and 81, respectively). (C) C660-evoked Ca^{2+} responses are specific to PAR3-expressing neurons, as demonstrated by the minimal Ca^{2+} responses from cultured PAR3$^{-/-}$ DRG neurons (n = 59). Fisher's exact test, ****p<0.0001, n represents the number of neurons imaged. (Panels D-E) C660 elicits similar response and selectivity in PAR3-induced HEK293 cells. Cell Index (CI) over time (hr) for (D) non-induced and (E) PAR3-induced HEK293 cells during and after treatment with varying concentrations of C660. CI was recorded every minute for four

hours (2 hours shown), with individual traces representing the average of four experiments from a single plate. Changes in peak values were used to construct (F) a concentration-response curve, with a calculated EC_{50} of 881 nM for human PAR3. Data points in (F) represent mean ± SEM, with n = 16, 16, 16, 15, 16, 3, 8, 6, and 4, respectively, in descending concentration, where n represents each peak difference for a given concentration.

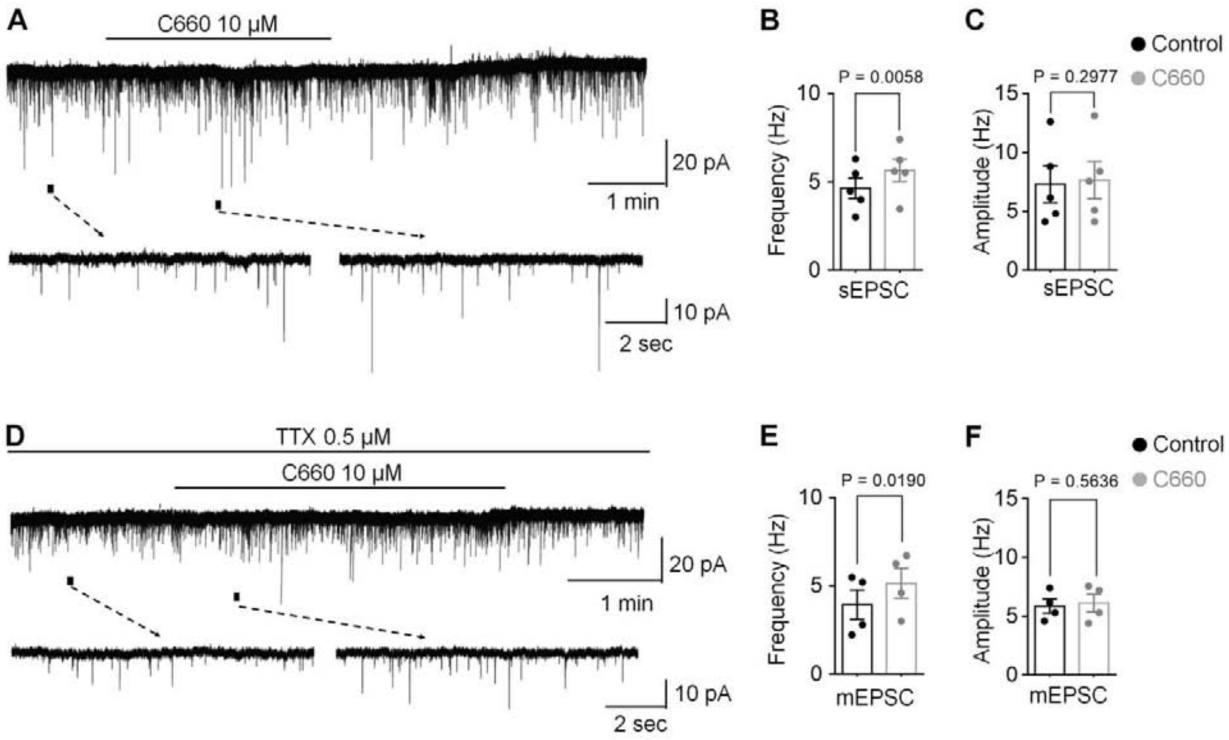

Figure 3. Peptidomimetic compound C660 acts presynaptically to increase dorsal horn excitatory synaptic transmission in spinal cord slices.

Whole-cell voltage-clamp recordings of lamina IIo neurons in lumbar segments of mouse spinal cord. (A) Representative traces of spontaneous excitatory postsynaptic currents (sEPSCs) before and after the application of C660 (10 μM). Lower: Enlarged traces of events for a period indicated by short bars. sEPSCs were recorded at a holding potential (V_H) of −70 mV in the presence of 10 μM picrotoxin and 2 μM strychnine. (B, C) sEPSC frequency (B) and sEPSC amplitude (C). Treatment of lumbar spinal cord slices with 10 μM C660 significantly increased the frequency but not the amplitude of recorded sEPSCs. n = 5 neurons/group. (D) Representative traces of miniature excitatory postsynaptic currents (mEPSCs) in lamina IIo neurons recorded in the presence of 10 μM picrotoxin, 2 μM strychnine, and 0.5 μM tetrodotoxin (TTX). Lower: enlarged traces of events for a period indicated by short bars. (E, F) mEPSC frequency (E) and mEPSC amplitude (F). C660 treatment (10 μM) in the presence of 0.5 μM tetrodotoxin (TTX) increased the frequency of mEPSCs with no change in amplitude (n = 4 neurons/group). Numerical data are represented as mean ± SEM. Statistical significance was determined as $P < 0.05$ using the paired Student's *t*-test. In all experiments, n refers to the number of the neurons studied. Only one neuron was recorded in each slice.

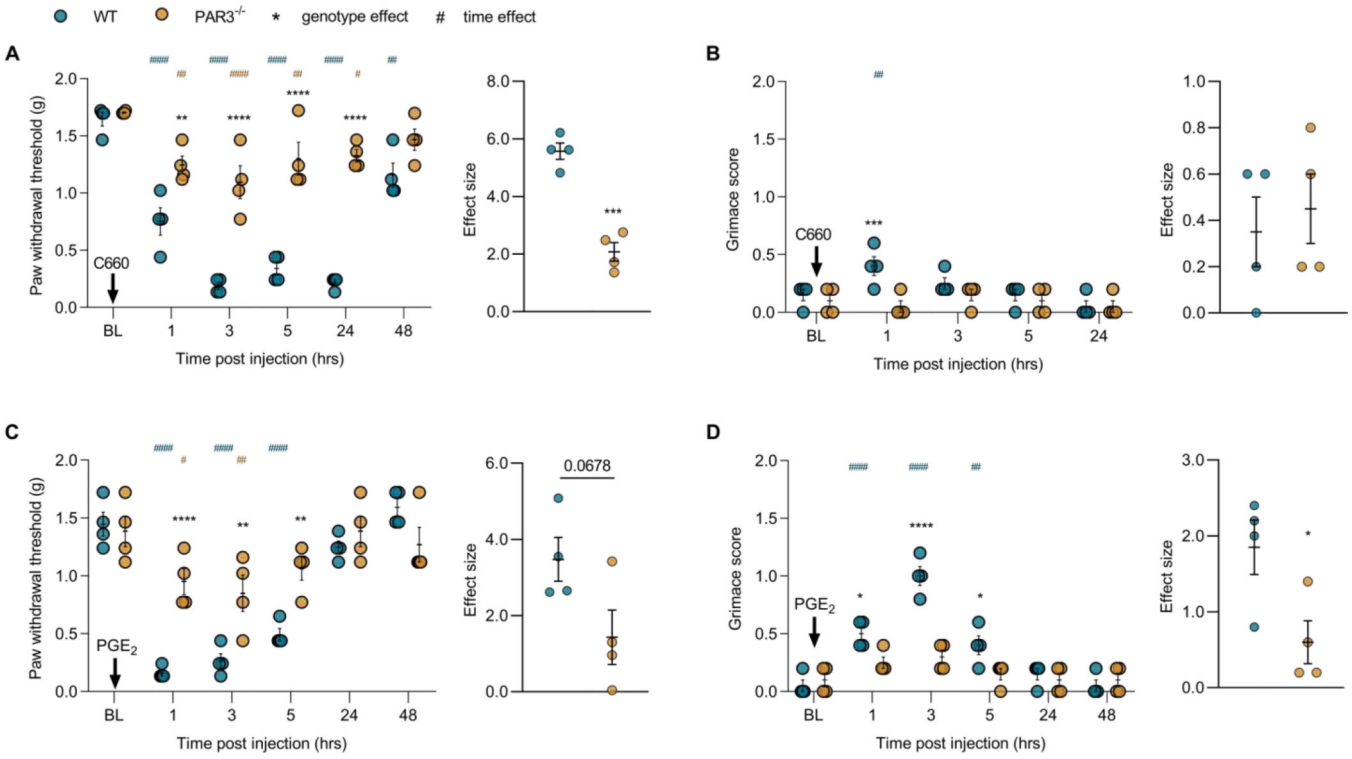

Figure 4. C660 acts on PAR3 to induce hyperalgesia and hyperalgesic priming.

WT and PAR3$^{-/-}$ mice were injected with C660 (30 pmol) intraplantarly after recording baseline (BL) measures for paw withdrawal threshold and grimacing. Mechanical and affective measures of pain were subsequently scored at 1, 3, 5, 24, and 48 hours post-injection. Effect sizes were calculated to compare the cumulative differences from baseline between the WT and PAR3$^{-/-}$ groups for the duration of 48 hrs post-injection. (A) PAR3 agonist, C660, significantly reduced paw withdrawal thresholds in the WT but not PAR3$^{-/-}$ group, with effects lasting up to 24 hrs post-injection (n = 4/group). (B) A transient increase in facial grimacing was observed with the WT cohort at the 1 hr time point. However, the overall effect size over a 24 hr period did not differ significantly between groups (n = 4/group). (C, D) Hyperalgesic priming was assessed by applying an initial stimulus of C660 (30 pmol) to the hind paw and allowing 14 days for complete recovery, after which PGE_2 (100 ng, i.pl) was applied. (C) Significant genotypic differences in hyperalgesic priming were observed at the 1, 3, and 5 hr time points and were resolved after 24 hrs. Cumulatively, PGE_2 hyperalgesia was partially attenuated in PAR3$^{-/-}$ cohort (n = 4/group). (D) PGE_2 produced a robust affective response in WT but not PAR3$^{-/-}$ mice. (Panels A-D) Data are expressed as mean ± SEM. Two-way ANOVA with Bonferroni's multiple comparisons *p<0.05, **p<0.01, ****p<0.0001. Unpaired t-test *p<0.05, ***p<0.001. Stars show significant differences between treatments or genotypes. Hashtags show differences by time, from baseline.

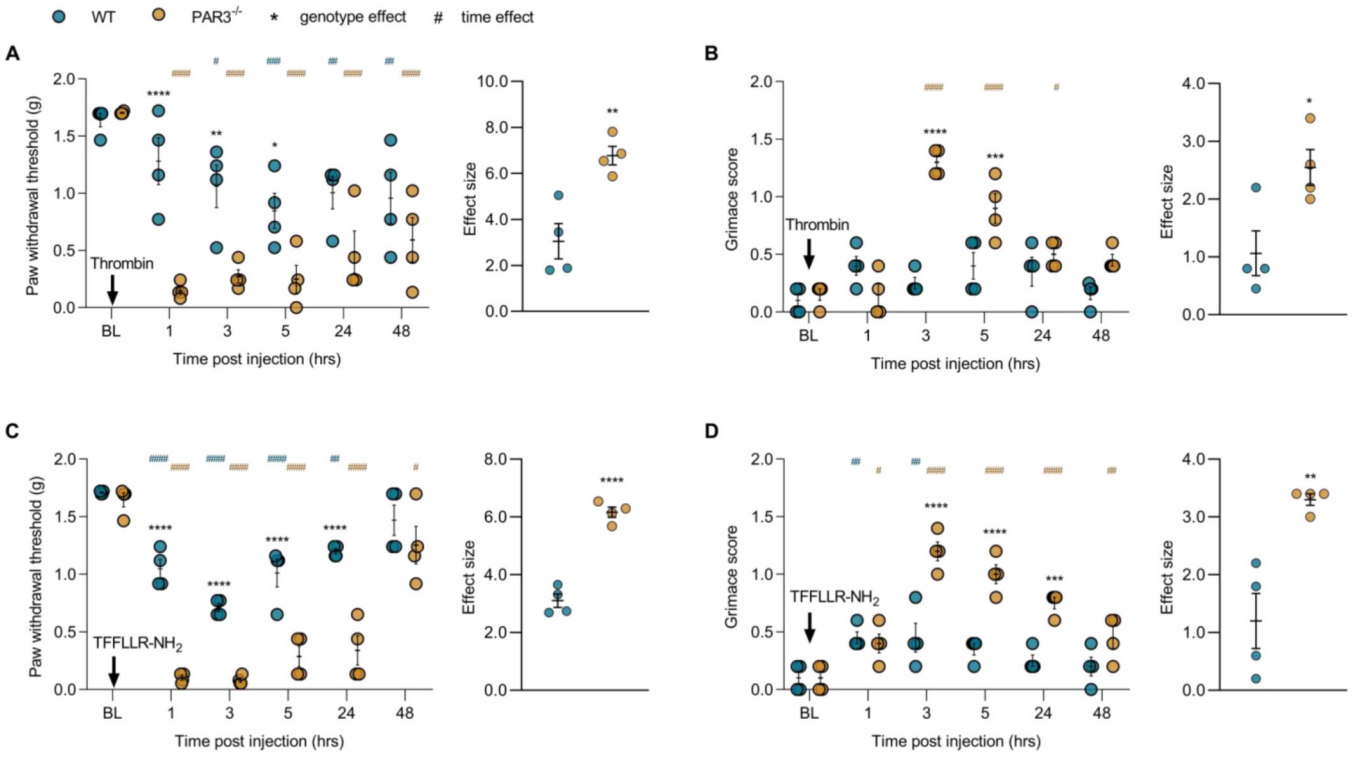

Figure 5. Pronociceptive effects of PAR1 agonists are increased and prolonged in PAR3$^{-/-}$ mice.

Thrombin or peptide PAR1 agonist, TFFLLR-NH_2, was administered intraplantarly into the hind paws of WT and PAR3$^{-/-}$ mice. Baseline (BL) recordings of mechanical thresholds and grimace scores were noted before administering either thrombin (10 units, i.pl) or TFFLLR-NH_2 (100 μg, i.pl). Paw withdrawal thresholds and grimace scores were then assessed 1, 3, 5, 24, and 48 hours post-injection. (A) Thrombin (10 units, i.pl) induced lasting mechanical hypersensitivity in both WT and PAR3$^{-/-}$ mice. However, the response to thrombin was significantly greater in PAR3$^{-/-}$ mice at 1, 3, and 5 hours post-injection (n = 4/group). (B) Thrombin (10 units, i.pl) significantly increased facial grimacing in PAR3$^{-/-}$ but not WT mice (n = 4/group). (C) Intraplantar injections of TFFLLR-NH_2 (100 μg) significantly reduced mechanical withdrawal thresholds in WT and PAR3$^{-/-}$ mice but was more marked in the latter group. Cumulatively, the genotypic differences throughout 48 hours post-injection were significant (n = 4/group). (D) TFFLLR-NH_2 (100 μg, i.pl) induced prolonged facial grimacing in PAR3$^{-/-}$ but not WT mice (n = 4/group). (Panels A-D) Data are expressed as mean ± SEM. Two-way ANOVA with Bonferroni's multiple comparisons *p<0.05, **p<0.01, ***p<0.001, ****p<0.0001. Unpaired t-test *p<0.05, **p<0.01, ****p<0.0001. Stars show significant differences between treatments or genotypes. Hashtags show differences by time, from baseline.

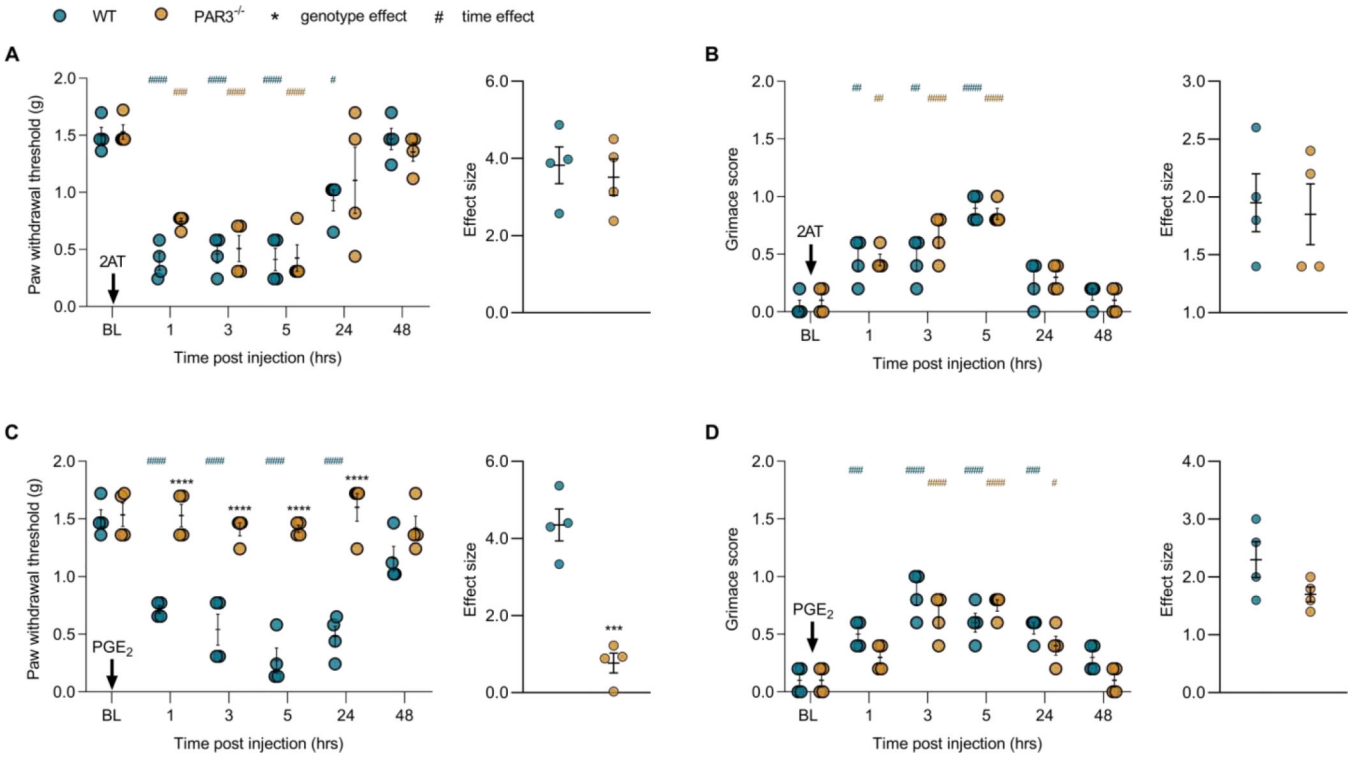

Figure 6. PAR2 agonist, 2AT, induces mechanical hypersensitivity and facial grimacing but not hyperalgesic priming in PAR3 deficient mice.

WT and PAR3$^{-/-}$ mice were injected with 2AT (30 pmol) into their hind paws, and then mechanical and affective measures of pain were recorded up to 48 hours. Effect sizes were calculated to compare the cumulative differences from BL over a 48 hr duration for the WT and PAR3$^{-/-}$ groups. 2AT injected into the hind paw significantly increased (A) mechanical hypersensitivity (B) and facial grimacing (n = 4/group) in both WT and PAR3$^{-/-}$ mice, with effects lasting up to 5 hours. (Panel C and D) WT and PAR3$^{-/-}$ mice were pretreated with 2AT (30 pmol, i.pl) and allowed to recover completely for 14 d. Following that, the mice received an injection of PGE_2 (100 ng) into the hind paw. Mechanical and affective measures of pain were assessed via von Frey testing and mouse grimace scale, respectively (n = 4/group). (C) Mechanical hyperalgesia after PGE_2 (100 ng) was robust in the WT group only. The time effect for the WT cohort was statistically significant up to 24 hours post PGE_2 injection. Unpaired t-test of the effect sizes reveals a significant genotype difference between WT and PAR3$^{-/-}$ groups (n = 4/group). (D) Facial grimacing was increased in both groups after PGE_2 (100 ng) injection (n = 4/group). (Panels A-D) Data are expressed as mean ± SEM. Two-way ANOVA with Bonferroni's multiple comparisons *p<0.05, **p<0.01, ***p<0.001, ****p<0.0001. Unpaired t-test ***p<0.001. Stars show significant differences between treatments or genotypes. Hashtags show differences by time, from baseline.

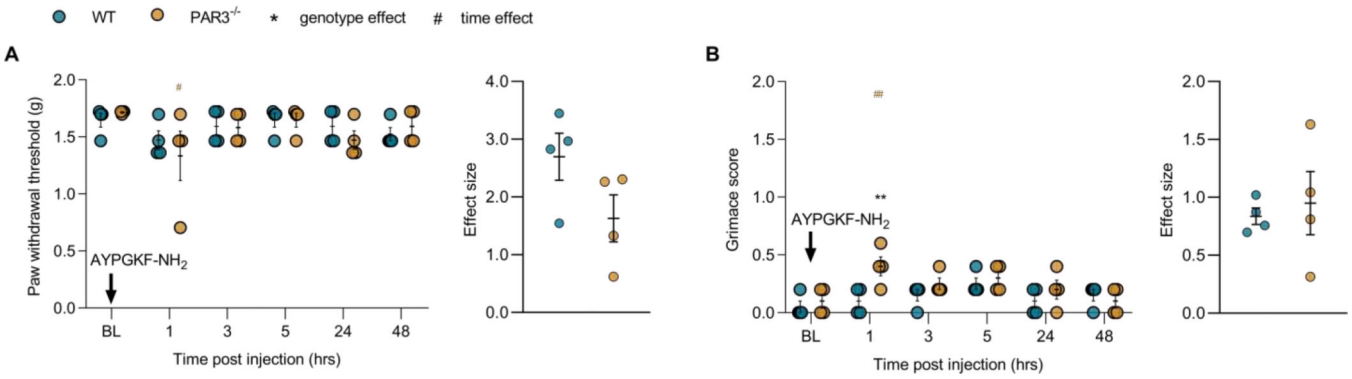

Figure 7. PAR4 agonist does not elicit mechanical or affective measures of pain.

100 μg of AYPGKF-NH_2, a PAR4 agonist, was injected into the hind paw of WT and $PAR3^{-/-}$ mice after recording baseline (BL) values. Von Frey and grimace tests were performed at 1, 3, 5, 24, and 48 hrs post-injection. (A) Paw withdrawal thresholds did not change significantly in both WT and $PAR3^{-/-}$ mice groups (n = 4/group). (B) Although facial grimacing was transiently increased with $PAR3^{-/-}$ at 1 hr post-injection, the cumulative time and genotype effects of AYPGKF-NH_2 (100 μg, i.pl) were insignificant (n = 4/group). (A, B) Data are expressed as mean ± SEM. Two-way ANOVA with Bonferroni's multiple comparisons *p<0.05, **p<0.01. Unpaired t-tests were performed for effect sizes. Stars show significant differences between treatments or genotypes. Hashtags show differences by time, from baseline.

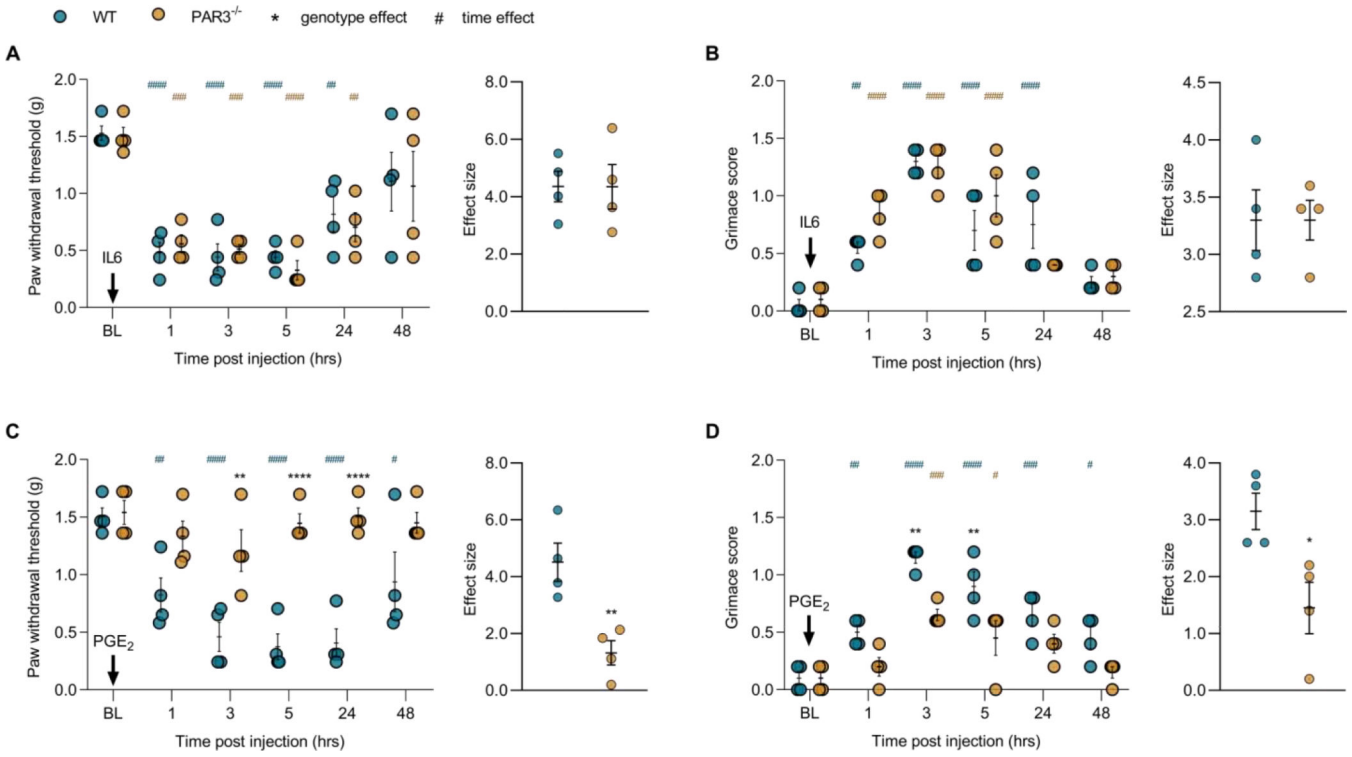

Figure 8. IL-6 elicits mechanical and affective pain responses but does not induce hyperalgesic priming in PAR3$^{-/-}$ mice.

(Panel A and B) WT and PAR3$^{-/-}$ mice received an injection of IL-6 (0.1 ng) into the hind paw after recording baseline (BL) values. Paw withdrawal thresholds and facial grimacing were scored at 1, 3, 5, 24, and 48 hrs post-injection. (A) Both WT and PAR3$^{-/-}$ mice demonstrated similar decreased mechanical withdrawal thresholds in response to IL-6 (0.1 ng, i.pl) (n = 4/group). (B) Likewise, IL6 (0.1 ng, i.pl) induced similar levels of facial grimacing in both cohorts (n = 4/group). (C, D) PGE_2 (100 ng) was administered intraplantarly in WT and PAR3$^{-/-}$ mice, 14 d after initial stimulation with IL-6 (0.1 ng, i.pl). PAR3$^{-/-}$ mice exhibit a deficiency in hyperalgesic priming; (C) paw withdrawal thresholds (n = 4/group), and (D) facial grimacing (n = 4/group) were not significantly affected by PGE_2 treatment in comparison to WT mice. (Panels A-D) Data are expressed as mean ± SEM. Two-way ANOVA with Bonferroni's multiple comparisons *p<0.05, **p<0.01, ***p<0.001, ****p<0.0001. Unpaired t-test *p<0.05, **p<0.01. Stars show significant differences between treatments or genotypes. Hashtags show differences by time, from baseline.